arXiv:2004.13532v1 [cs.NE] 28 Apr 2020

SPIKING MACHINE INTELLIGENCE

WHAT WE CAN LEARN FROM BIOLOGY AND HOW SPIKING NEURAL NETWORKS CAN HELP TO IMPROVE MACHINE LEARNING

Richard C. Gerum
Biophysics Group, Department of Physics
Friedrich Alexander University Erlangen-Nürnberg (FAU), Germany

Achim Schilling
Experimental Otolaryngology,
Neuroscience Lab, University Hospital Erlangen, Germany
Cognitive Computational Neuroscience Group
at the Chair of English Philology and Linguistics,
Friedrich-Alexander University Erlangen-Nürnberg (FAU), Germany

June 5, 2022

Corresponding author:
Dr. Achim Schilling
Neuroscience Group
Experimental Otolaryngology
Friedrich-Alexander University of Erlangen-Nürnberg
Waldstrasse 1
91054 Erlangen, Germany
Phone: +49 9131 8543853
E-Mail: achim.schilling@uk-erlangen.de

ABSTRACT

Up to now, modern Machine Learning is based on fitting high dimensional functions to enormous data sets, taking advantage of huge hardware resources.

We show that biologically inspired neuron models such as the Integrate-and-Fire (LIF) neurons provide novel and efficient ways of information encoding. They can be integrated in Machine Learning models, and are a potential target to improve Machine Learning performance. Thus, we systematically analyze the LIF neuron. We start by deriving simple integration equations to which even a gradient can be assigned. Additionally, we prove that a Long-Short-Term-Memory unit can be tuned to show similar spiking properties. Additionally, LIF units are applied to an image classification task, trained with backpropagation.

With this study we want to contribute to the current efforts to enhance Machine Intelligence by integrating principles from biology.

1 Introduction

The interest in „Neuroscience inspired AI“ has rapidly grown over the last years (Hassabis et al., 2017). What is the reason for this development?

Although traditional Machine Learning algorithms have been massively improved by huge data sets (Russakovsky et al., 2015) and modern hardware components (Steinkraus et al., 2005; Sheng and Zhou, 2017), certain issues remain unsolved by these algorithms. Up to now, these algorithms are—in contrast to our brain—highly specialized on a given task. We were not yet able to develop algorithms with general intelligence (Shevlin et al., 2019; Pontes-Filho and Nichele, 2019). Our nervous system has the ability to perform sensory tasks with enormous precision, such as the detection of very low stimuli in the eye (Field et al., 2019; Rieke and Baylor, 1998) or very small pressure differences in the ear and on the other hand is able to process and understand complex story plots (Mar, 2004; Tenenbaum et al., 2006). Thus, we do not need huge hardware components but are limited to approximately 10^{11} neurons (Herculano-Houzel, 2009), which perform these tasks in a very efficient way.

Information can be processed faster and more efficiently in the brain, as spiking neural networks can encode data in different spatio-temporal patterns (Thorpe et al., 2001; Perkel and Bullock, 1968; Krauss et al., 2018; Gross and Kowalski, 1999). Thus, the brain does not simply count spikes (rate codes) but exploits the temporal dynamics of these spikes (Koopman et al., 2003) and uses spontaneous spiking and neural noise to enhance sensory processing (Schilling et al., 2020; Krauss et al., 2017, 2016).

Different biological inspired neuron models have been developed (Hodgkin and Huxley, 1952; Izhikevich and FitzHugh, 2006), but they are rarely integrated in Machine Learning applications.

We show how the biologically inspired Leaky-Integrate-and-Fire (LIF) neurons (Burkitt, 2006) can be applied in Machine Learning models to potentially improve performance and increase interpretability on the one hand ("Neuroscience inspired AI" (Hassabis et al., 2017), “Machine Behavior”, (Rahwan et al., 2019)) and to create models for biology on the other hand (“Cognitive Computational Neuroscience”, (Kriegeskorte and Douglas, 2018)).

Thus in this paper:

- We visualize and explain the function of LIF neurons.
- We prove that peephole Long-Short-Term Memory (LSTM) cells (Hochreiter and Schmidhuber, 1997; Gers and Schmidhuber, 2000, 2001; Yang et al., 2018) can be driven in a LIF mode.
- We show that LIF units can be trained using backpropagation.
- We apply a hybrid neural network on image classification and prove the validity of our findings.

2 Leaky Integrate and Fire Neurons (LIF)

2.1 The LIF Unit

As described above the Leaky-Integrate-and-Fire (LIF) neuron model is a simple spiking neuron model based on one single differential equation. The idea is that the neuron sums up all input currents, increases its membrane potential and produces a spike if a certain threshold is reached. The leak term causes a continuous decrease of the membrane potential and thus prevents long range correlations.

The leaky integrate and fire (LIF) neuron’s(Koch et al., 1998) membrane potential V_m is described by the following differential equation:

$$I(t) - \frac{V_\mathrm{m}(t)}{R_\mathrm{m}} = C_\mathrm{m} \cdot \dot{V}_\mathrm{m}(t) \tag{1}$$

with the input $I(t)$, the membrane resistance R_m, and the capacity C_m.

When the membrane potential exceeds a threshold V_th a spike in form of a delta function $\delta(t)$ is emitted and the membrane potential is reset to 0.

To simulate the response of a LIF neuron, this differential equation has to be integrated. The simplest integration method is the Euler integration(Atkinson, 1989). We choose this method for its numerical simplicity.

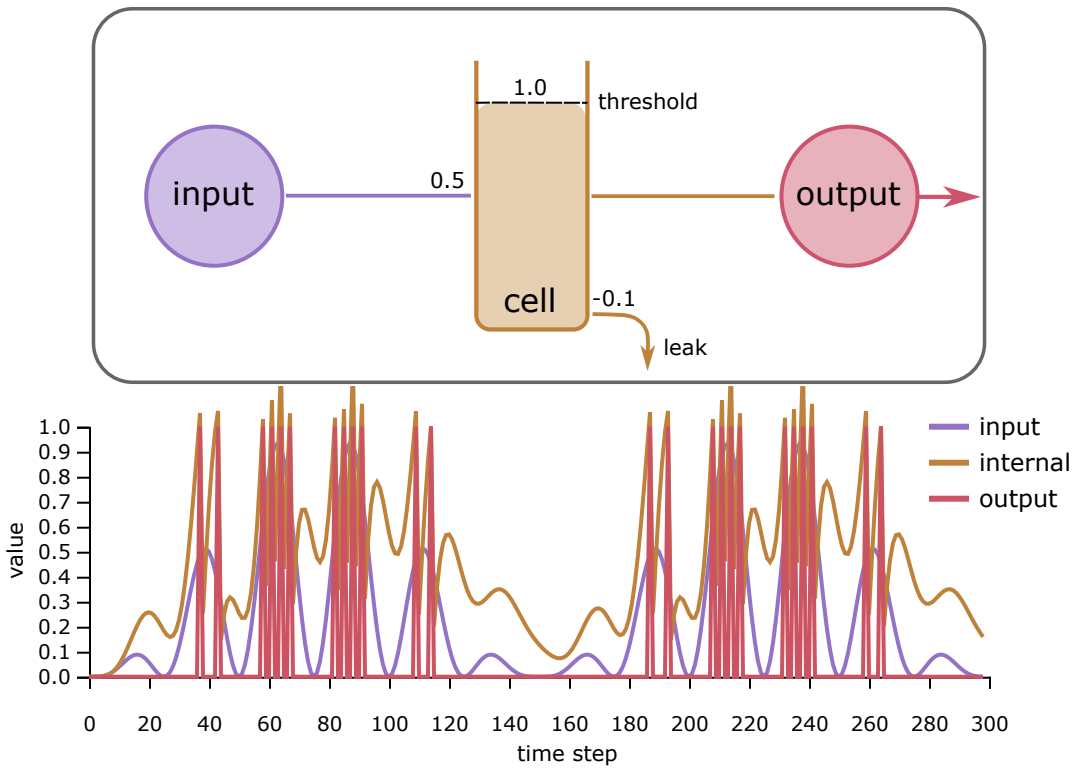

Figure 1: **The response of the leaky integrate and fire neurons.** The cell (orange) integrates the input (purple) until the internal state exceeds the threshold. Then it outputs a spike (red). The leak term lets the cell state decay over time.

First, we solve the equation for $\dot{V}_{\mathrm{m}}(t)$

$$\dot{V}_{\mathrm{m}}(t) = \frac{I(t)}{C_{\mathrm{m}}} - \frac{V_{\mathrm{m}}(t)}{R_{\mathrm{m}} C_{\mathrm{m}}} \tag{2}$$

and convert the differential equation to an Euler step:

$$V_{t+1} = V_t + \left(C_{\mathrm{m}}^{-1} \cdot x_t - V_t \cdot R_{\mathrm{m}}^{-1} C_{\mathrm{m}}^{-1}\right) \cdot \Delta t \tag{3}$$

with the time step delta Δt, and the $I(t)$ now named x_t.

We extend the update equation to include the spiking when the threshold has been reached and the resetting of V_{t+1} after the spike.

$$\tilde{V}_{t+1} = V_t + \left(C_{\mathrm{m}}^{-1} \cdot x_t - V_t \cdot R_{\mathrm{m}}^{-1} C_{\mathrm{m}}^{-1}\right) \cdot \Delta t \tag{4}$$

$$y_{t+1} = \Theta(\tilde{V}_{t+1} - V_{\mathrm{thresh}}) \qquad \text{spiking} \tag{5}$$

$$V_{t+1} = V_{\mathrm{m}} \cdot \Theta(-\tilde{V}_{t+1} + V_{\mathrm{thresh}}) \qquad \text{resetting} \tag{6}$$

Here $\Theta(x)$ is the Heaviside step function.

For our visualization above we have used the following parameters:

$$C_{\mathrm{m}}^{-1} \Delta t = w_{\mathrm{input}} = 0.5 \tag{7}$$

$$R_{\mathrm{m}}^{-1} C_{\mathrm{m}}^{-1} \cdot \Delta t = w_{\mathrm{leak}} = 0.1 \tag{8}$$

$$V_{\mathrm{thresh}} = 1.0 \tag{9}$$

The update rule of the LIF unit can be summarized as follows:

$$V_t = w_{\mathrm{input}} \cdot x_t + (1 - w_{\mathrm{leak}}) \cdot V_{\mathrm{t-1}} \cdot \Theta(V_{\mathrm{thresh}} - V_{\mathrm{t-1}}) \tag{10}$$

$$y_t = \Theta(V_t - V_{\mathrm{thresh}}) \tag{11}$$

These equations can be used to analytically calculate the firing rates of the LIF neurons. The firing rates are an important property for many Machine Learning algorithms (Dominguez-Morales et al., 2016).

2.2 Firing Rates

We will analytically calculate the number of timesteps with a constant input I which are necessary to provoke a spike.

At time t_0 we start with $V_{t_0} = w_{input} \cdot I$ and apply the update rule for LIF units as shown above:

$$V_{t_n} = w_{\text{input}} \cdot I + (1 - w_{\text{leak}}) \cdot V_{t_n - 1} \tag{12}$$

The implicit description of V_{t_n} can be written in an explicit manner.

$$V_{t_n} = \sum_{i=0}^{n} (1 - w_{\text{leak}})^i \cdot w_{\text{input}} \cdot I \tag{13}$$

The criterion for a spike is: $V_{t_n} \geq V_{\text{thresh}}$. Thus, the following inequation has to be solved:

$$V_{\text{thresh}} \leq \sum_{i=0}^{n} (1 - w_{\text{leak}})^i \cdot w_{\text{input}} \cdot I \tag{14}$$

$$\leq w_{\text{input}} \cdot I \cdot \sum_{i=0}^{n} (1 - w_{\text{leak}})^i \quad \text{with} \sum_{i=0}^{n} a^i = \frac{a^{n+1} - 1}{a - 1} \tag{15}$$

$$\leq w_{\text{input}} \cdot I \cdot \frac{(1 - w_{\text{leak}})^{n+1} - 1}{-w_{\text{leak}}} \tag{16}$$

$$-\frac{V_{\text{thresh}}}{I} \cdot \frac{w_{\text{leak}}}{w_{\text{input}}} + 1 \geq (1 - w_{\text{leak}})^{n+1} \tag{17}$$

$$\ln\left(-\frac{V_{\text{thresh}}}{I} \cdot \frac{w_{\text{leak}}}{w_{\text{input}}} + 1\right) \geq (n+1) \cdot \ln(1 - w_{\text{leak}}) \tag{18}$$

$$n \geq \frac{\ln\left(1 - \frac{V_{\text{thresh}}}{I} \cdot \frac{w_{\text{leak}}}{w_{\text{input}}}\right)}{\ln(1 - w_{\text{leak}})} - 1 \tag{19}$$

$$\tag{20}$$

This results in the number of timesteps until the next spike event.

$$n = \text{ceil}\left(\frac{\ln\left(1 - \frac{V_{\text{thresh}}}{I} \cdot \frac{w_{\text{leak}}}{w_{\text{input}}}\right)}{\ln(1 - w_{\text{leak}})} - 1\right) \tag{21}$$

Note, for $w_{\text{leak}} = 0$ this simplifies to:

$$n = \text{ceil}\left(\frac{V_{\text{thresh}}}{w_{\text{input}} \cdot I}\right) \tag{22}$$

The equation shows that n is a nonlinear function of w_{leak} and w_{input} and thus a simple downregulation of w_{leak} cannot be compensated by a downregulation of w_{input}. On the other hand, V_{thresh} can be fixed to 1 without loss of generality as a change of V_{thresh} can be absorbed in w_{input}.

The spiking only occurs at all if the input exceeds the input threshold:

$$I_{\text{min}} = \frac{V_{\text{thresh}} \cdot w_{\text{leak}}}{w_{\text{input}}} \tag{23}$$

Smaller inputs lead to a divergence of the n as the cell state decays faster than it is resupplied by the input.

The equation for the input threshold I_{minh} shows that the input threshold is only non-zero if the neuron is "leaky", e.g. has a leak parameter $w_{\text{leak}} \neq 0$.

The fact that the two parameters w_{leak} and w_{input} have different effects on the spike rate, and cannot be trivially combined to one parameter, training of these two parameters can help to extract interesting features from the input data.

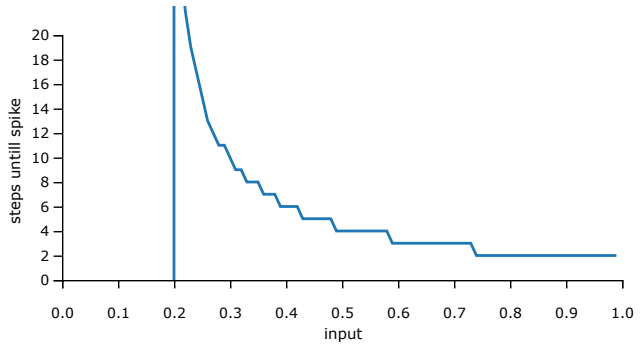

Figure 2: **Average number of timesteps needed for spike (corresponds to inverse spike rate).** The curve (blue) shows the steps it takes for the neuron to spike when it receives a constant input ($w_{\text{input}} = 0.5$, $w_{\text{leak}} = 0.1$).

2.3 Smoothing of the Theta function

One common problem in Machine Learning is the so called vanishing gradient. The gradient descent algorithm does not converge to a minimum if there is no gradient, which can be used to minimize the loss function. For LIF neurons this problem is obvious as the gradient of the Heaviside function is always 0 (except directly at 0). One potential solution for that problem is to smoothen the Heaviside function $\Theta(x)$ by replacing it with a sigmoid function $\sigma(x)$.

$$\tilde{\Theta}(x) = \sigma(x/\alpha_{\text{smooth}}) \tag{24}$$

with a smoothing factor α_{smooth}. For the limit $\alpha_{\text{smooth}} \to 0$ the function converges to the Heaviside function.

The equations for the LIF unit contains two Θ functions that can be smoothed separately, as shown in the next figure.

$$V_t = w_{\text{input}} \cdot x_t + (1 - w_{\text{leak}}) \cdot V_{\text{t}-1} \cdot \tilde{\Theta}_2(V_{\text{thresh}} - V_{\text{t}-1}) \tag{25}$$

$$y_t = \tilde{\Theta}_1(V_t - V_{\text{thresh}}) \tag{26}$$

In paragraph "Calculation of the Gradient" we will show that there is a mathematical trick to resolve this difficulty.

3 Spiking Long Short-Term Memory Units (LSTM)

In the next paragraph, we show that LIFs and LSTM units are tightly connected, when the paramters of the LSTMS units are tuned in a certain way. This connection can help to represent LIF units in already established Machine learning frameworks such as Keras(Chollet, 2018). Furthermore, it is possible to exploit the experiences with and the properties of the LSTM units. The long short-term memory (LSTM)(Hochreiter and Schmidhuber, 1997) units are among the most used memory units in recurrent neural networks. They share certain similarities with the LIF neurons such as the fact that they have an internal memory — "the membrane potential". In the following, we show that LSTM units and LIF neurons are very similar, when the parameters are tuned correctly. We start with a standard implementation of a LSTM unit with peephole connections (Gers and Schmidhuber, 2000, 2001; Yang et al., 2018).

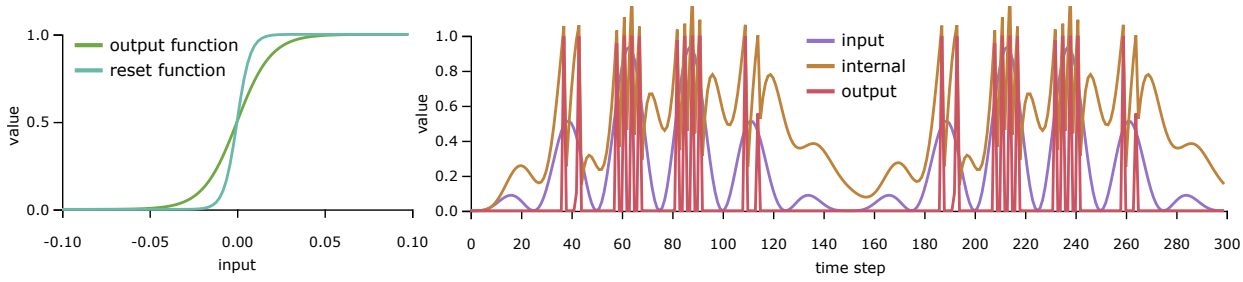

Figure 3: **Response of the LIF unit with different smoothing parameters.** The output function Θ_1 ($\alpha_{\text{smooth1}} = 0.010$) can be smoothed independently of the reset function Θ_2 ($\alpha_{\text{smooth2}} = 0.004$). The input is summed until the threshold is reached. Then the spike is outputted using Θ_1 and the internal state is resetted using Θ_2.

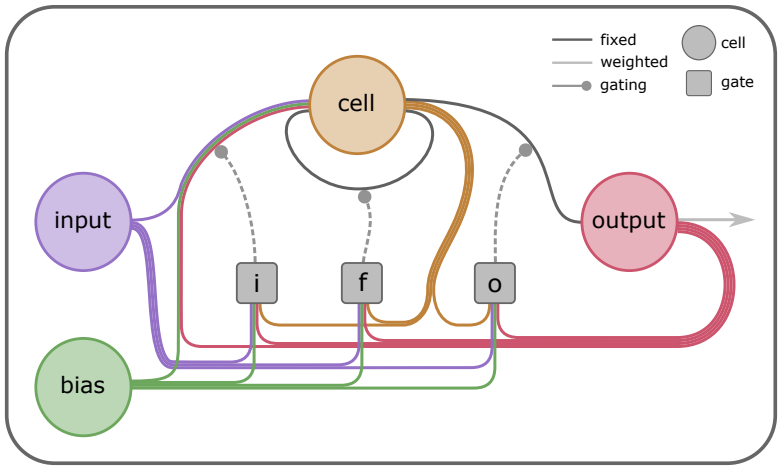

Figure 4: **Architecture of a peephole LSTM.** The input, bias, and output are connected to the input of the cell and all three gates (input, forget, output). The cell has peephole connections to the gates.

The figure can be translated to the following equations.

$$V_t = (b_{\text{input}} + w_{\text{input}} \cdot x_t + w_{\text{output}} \cdot y_{t-1}) \tag{27}$$
$$\cdot\sigma(b_1 + f_{\text{input1}} \cdot x_t + f_{\text{cell1}} \cdot V_{t-1} + f_{\text{output1}} \cdot y_{t-1}) \tag{28}$$
$$+V_{t-1} \cdot \sigma(b_2 + f_{\text{input2}} \cdot x_t + f_{\text{cell2}} \cdot V_{t-1} + f_{\text{output2}} \cdot y_{t-1}) \tag{29}$$
$$y_t = V_{t-1} \cdot \sigma(b_3 + f_{\text{input3}} \cdot x_t + f_{\text{cell3}} \cdot V_{t-1} + f_{\text{output3}} \cdot y_{t-1}) \tag{30}$$

$f_{\text{cell1,2,3}}$ are the so called peephole connections. The general LSTM can be simplified by the removal of unneeded connections. $f_{\text{input1,2,3}} = 0$, $f_{\text{cell1}} = 0$, $b_2 = 0$, $f_{\text{cell2}} = 0$

$$V_t = w_{\text{input}} \cdot x_t \cdot \sigma(b_1) + V_{t-1} \cdot \sigma(b_2 + f_{\text{output2}} \cdot y_{t-1}) \tag{31}$$
$$y_t = V_{t-1} \cdot \sigma(f_{\text{cell3}} \cdot V_{t-1} + b_3) \tag{32}$$

Now, we tune the LSTM so that it resembles a LIF.

- $b_1 = 100 \gg 0$, thus $\sigma(b_1) \approx 1$, keep the **input gate** always open,
- $b_2 = \sigma^{-1}(1 - w_{leak})$, open the forget so that it acts as a **leak term**,
- $f_{\text{output2}} = -200 \ll 0$, **reset** the state after a spike,
- $f_{cell3} = 200 \gg 0$, $b_3 = -f_{\text{cell3}}$, mimic a theta function to open the **output** when the state exceeds the threshold of 1.

Thus, the terms of the LSTM can be written as follows:

$$V_t = w_{\text{input}} \cdot x_t \cdot \sigma(b_1) + V_{t-1} \cdot \sigma(\sigma^{-1}(1 - w_{\text{leak}}) + f_{\text{output2}} \cdot y_{t-1}) \tag{33}$$
$$y_t = V_{t-1} \cdot \sigma(f_{\text{cell3}} \cdot (V_{t-1} - 1)) \tag{34}$$

If we now consider the fact that:

$$\sigma(\alpha \cdot x) \approx \begin{cases} 1 & \text{for } x > 0 \text{ and } \alpha \gg 0 \\ 0 & \text{for } x < 0 \text{ and } \alpha \gg 0 \end{cases} \tag{35}$$
$$\sigma(\alpha \cdot x) \approx \Theta(x) \tag{36}$$

We end up with the approximated terms:

$$V_t = w_{input} \cdot x_t + V_{t-1} \cdot \sigma(\sigma^{-1}(1 - w_{\text{leak}}) + f_{\text{output2}} \cdot y_{t-1}) \tag{37}$$
$$y_t = V_{t-1} \cdot \Theta(V_{t-1} - 1) \tag{38}$$

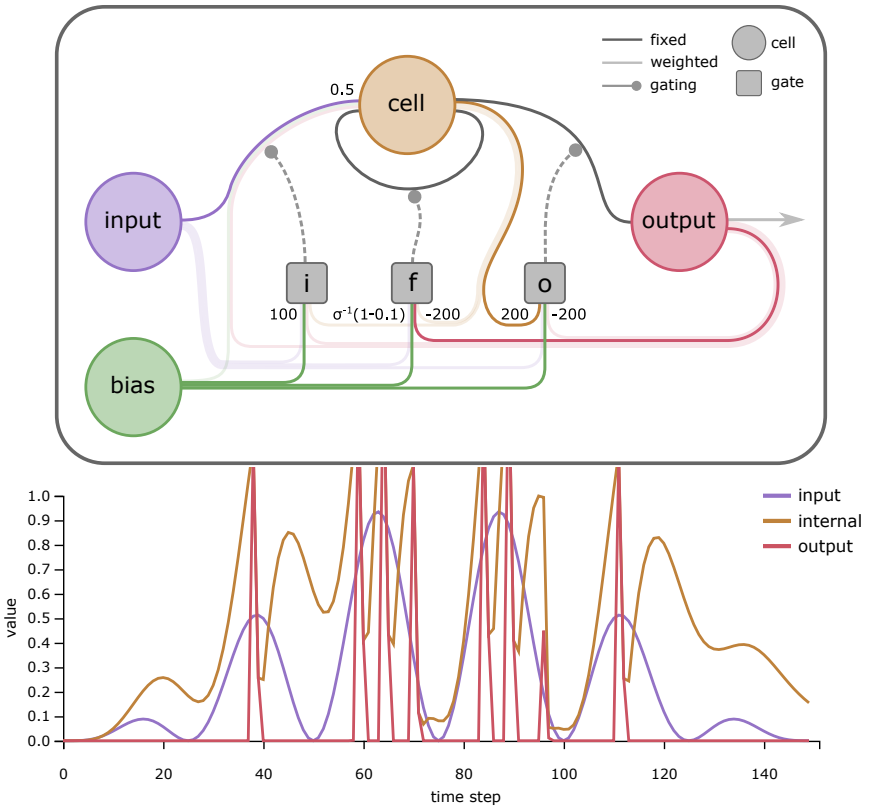

Figure 5: **The response of the LSTM unit with peep-hole connection.** The cell's internal state accumulates the input. If the state reaches 1, the output gate opens an the unit's output produces a "spike". Investigate also the peak state and the post peak state. These states can be similarly observed in LIF neurons.

Thus, we know $y_t \approx 0$ or $y_t \approx 1$ and $f_{\text{output2}} = -200 \ll 0$

$$\sigma(\sigma^{-1}(1 - w_{\text{leak}}) + f_{\text{output2}} \cdot y_{t-1}) \approx \begin{cases} (1 - w_{\text{leak}}) & \text{for } y_{t-1} = 0 \\ 0 & \text{for } y_{t-1} = 1 \end{cases} \tag{39}$$

$$\sigma(\sigma^{-1}(1 - w_{\text{leak}}) + f_{\text{output2}} \cdot y_{t-1}) \approx (1 - w_{\text{leak}}) \cdot \Theta(1 - y_{t-1}) \tag{40}$$

The use of this approximation leads to following approximation of the peephole LSTM:

$$V_t = w_{\text{input}} \cdot x_t + V_{t-1} \cdot (1 - w_{\text{leak}}) \cdot \Theta(1 - y_{t-1}) \tag{41}$$

$$y_t = V_{t-1} \cdot \Theta(V_{t-1} - 1) \tag{42}$$

The output y_t is unfortunately no real spiking output. Despite the fact that the Θ function prevents a continuous output, the suprathreshold output is a continuous value in contrast to what we see in LIF neurons. However, in first order approximation the output can be seen as spiking, as just in the moment of the spike where $V_{t-1} > 1$, the value of V_{t-1} is resetted. Thus, in the moment of the spike, V_{t-1} can be regarded as $V_{t-1} \approx 1$.

Despite these limitations, the LSTM units can nevertheless produce spiking behavior as we show in the figure below.

4 Deep Learning with LIF Neurons

4.1 LIF Neurons and Multidimensional Data

When the LIF neurons are applied to multi-dimensional data such as an image an efficient representation is needed to optimize LIF neurons for our standard hardware and software architectures. The image, which we feed to the LIF units has N rows and M columns. However, we regard the image as serial data set, where the time axis corresponds to the

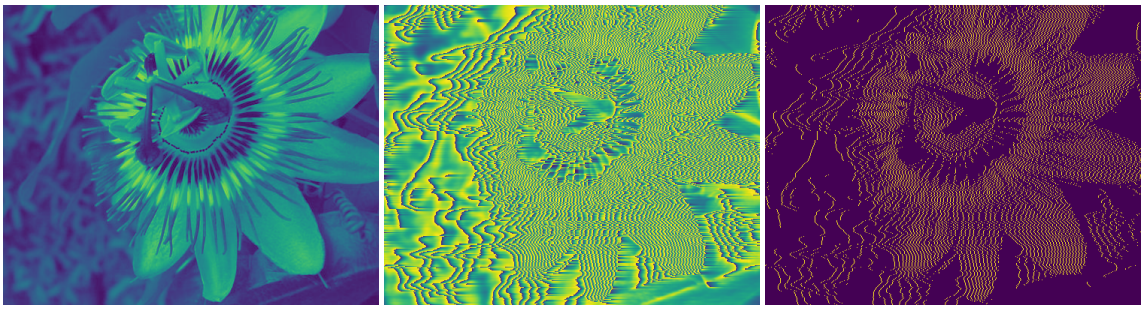

Figure 6: **Image processed columnwise by a LIF layer.** The figureshows the input (left), internal state (middle) the output (right) of the LIF layer.

x-axis of the image. Thus, the input of the LIF neurons consists of an N-dimensional vector for each of the M time steps. Therefore, also V_t and y_t are N-dimensional vectors. The following illustration shows the results of one LIF unit applied to an image of a passion flower blossom.

$$V_t = w_{\text{input}} \cdot x_t + (1 - w_{\text{leak}}) \cdot V_{\text{t}-1} \cdot \Theta(V_{\text{thresh}} - V_{\text{t}-1}) \tag{43}$$

$$y_t = \Theta(V_t - V_{\text{thresh}}) \tag{44}$$

The model can be extended by the use of several LIF units with different w_{input} and w_{leak}. This would make w_{input} and w_{leak} a vector instead of a scalar and the scalar product would transform into a tensor product. This is an efficient representation, which can easily be optimized for GPUs.

4.2 Calculation of the Gradient

The standard method to train neural networks on a classification task is to minimize a loss function $L(y_{\text{out}}, y_{\text{desired}})$. It is a measure of the dissimilarity between the desired output and the output of the neural network y_{out} calculated by forward propagation. For example in a classification task with a softmax output, the loss function usually is the cross-entropy. This loss function is minimized using the gradient descent algorithm.

The gradient descent works by adding the negative gradient multiplied with the learning rate γ to the weights, which have to be optimized.

$$\Delta W = -\gamma \cdot \frac{\mathrm{d}L}{\mathrm{d}W} \tag{45}$$

To illustrate the calculation of the gradient, we use an example architecture, consisting of two fully-connected layers and a LIF layer in between.

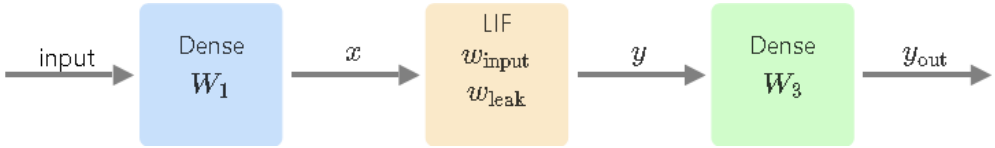

To calculate the update of the weights W_1, we have to calculate the gradient $\frac{\mathrm{d}L}{\mathrm{d}W_1}$.

$$\frac{\mathrm{d}L}{\mathrm{d}W_1} = \frac{\partial L}{\partial y_{\text{out}}} \cdot \frac{\partial y_{\text{out}}}{\partial y} \cdot \frac{\partial y}{\partial x} \cdot \frac{\mathrm{d}x}{\mathrm{d}W_1} \tag{46}$$

The term $\frac{\partial y}{\partial x}$ is the derivative of the LIF output as a function of the LIF input. If this derivative is 0 the weights of the first layer W_1 cannot be trained.

Let's have a look at the equations for the LIF unit:

$$V_t = w_{\text{input}} \cdot x_t + (1 - w_{\text{leak}}) \cdot V_{\text{t}-1} \cdot \Theta_2(V_{\text{thresh}} - V_{\text{t}-1}) \tag{47}$$

$$y_t = \Theta_1(V_t - V_{\text{thresh}}) \tag{48}$$

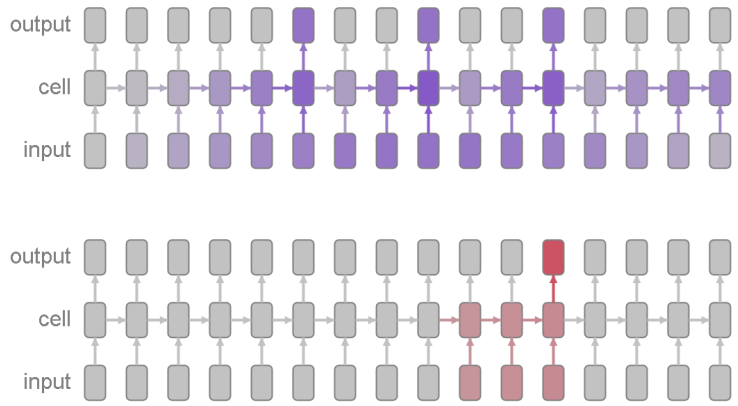

Figure 7: **The response and gradient of a LIF cell.** Each column represents one time step. The color saturation denotes the value of the cells. The lower image denote the back propagated error from the red time step. The derivatives are defined as follows: $\Theta_1'(x) = 1$, $\Theta_2'(x) = 0$.

Unfortunately, the spike outputs are generated using a Heaviside step function, whose gradient is 0. Thus, no gradient can enter or pass the LIF cell.

As discussed above, one possibility would be to smooth the theta functions. But a more elegant solution, that does not affect the forward pass, is to just redefine the gradient of the LIF unit. Let's have a look at the derivative of the equations with respect to the inputs.

$$\frac{\partial y_t}{\partial x_t} = \frac{\partial y_t}{\partial V_t}\frac{\partial V_t}{\partial x_t} = \Theta_1'(V_t - V_{\text{thresh}}) \cdot w_{\text{input}} \tag{49}$$

$$\frac{\partial y_t}{\partial x_{t-1}} = \frac{\partial y_t}{\partial V_t}\frac{\partial V_t}{\partial V_{t-1}}\frac{\partial V_{t-1}}{\partial x_{t-1}} \tag{50}$$

$$= \Theta_1'(V_t - V_{\text{thresh}}) \cdot (1 - w_{\text{leak}}) \cdot [\Theta_2(V_{\text{thresh}} - V_{t-1}) \cdot w_{\text{input}} + V_{t-1} \cdot \Theta_2'(V_{\text{thresh}} - V_{t-1}) \cdot w_{\text{input}}] \tag{51}$$

If we define $\Theta_2'(x) = 0$, then the expression for an arbitrary derivative for a past x is:

$$\frac{\partial y_t}{\partial x_{t-n}} = \Theta_1'(V_t - V_{\text{thresh}}) \cdot w_{\text{input}}(1 - w_{\text{leak}})^n \prod_{i=1}^{n} \Theta_2(V_{\text{thresh}} - V_{t-1}) \tag{52}$$

One can see that the crucial part is here the function Θ_1 that prevent with its derivative of 0 any gradient. Therefore, we redefine the gradient of Θ_1 to be 1 and keep the gradient of Θ_2 as 0.

The following figure illustrates how these definitions control the flow of the gradient.

It can be seen that the gradient now enters the cell (as $\Theta_1' = 1$) and propagates to all input units that contributed to the spike but does not penetrate to inputs that contributed to the previous spike (as $\Theta_2' = 0$).

We have shown that our gradient definition allows errors to pass the LIF neurons to pre-connected layers.

Now, we calculate the gradients for the LIFs parameters, as these parameters should also be trainable. Therefore, we calculate the derivative of the LIF output with respect to w_{input} and w_{leak}. Note that we still define $\Theta_2'(x) = 0$.

The gradient with respect to w_{input}:

$$\begin{aligned}
&\frac{\mathrm{d}y_t}{\mathrm{d}w_{\text{input}}} = \frac{\partial y_t}{\partial V_t}\left(\frac{\partial V_t}{\partial w_{\text{input}}} + \frac{\partial V_t}{\partial V_{t-1}}\frac{\mathrm{d}V_{t-1}}{\mathrm{d}w_{\text{input}}}\right) = \\
&\frac{\partial y_t}{\partial V_t}\left\{\frac{\partial V_t}{\partial w_{\text{input}}} + \frac{\partial V_t}{\partial V_{t-1}}\left[\frac{\partial V_{t-1}}{\partial w_{\text{input}}} + \frac{\partial V_{t-1}}{\partial V_{t-2}}\left(\frac{\partial V_{t-2}}{\partial w_{\text{input}}} + \frac{\partial V_{t-2}}{\partial V_{t-3}}\frac{\mathrm{d}V_{t-3}}{\mathrm{d}w_{\text{input}}}\right)\right]\right\} = \\
&\Theta_1'(V_t - V_{\text{thresh}}) \cdot \Big[x_t + (1 - w_{\text{leak}})\Theta_2(V_{\text{thresh}} - V_{t-1})x_{t-1} + \\
&(1 - w_{\text{leak}})^2\Theta_2(V_{\text{thresh}} - V_{t-1})\Theta_2(V_{\text{thresh}} - V_{t-2})x_{t-2} + \\
&(1 - w_{\text{leak}})^3\Theta_2(V_{\text{thresh}} - V_{t-1})\Theta_2(V_{\text{thresh}} - V_{t-2})\Theta_2(V_{\text{thresh}} - V_{t-2})\frac{\mathrm{d}V_{t-3}}{\mathrm{d}w_{\text{input}}}\Big] = \\
&\Theta_1'(V_t - V_{\text{thresh}}) \cdot \Big[x_t + \textstyle\sum_{n=1}^{N} x_{t-n}(1 - w_{\text{leak}})^n \cdot \prod_{i=1}^{n}\Theta_2(V_{\text{thresh}} - V_{t-i})\Big]
\end{aligned} \tag{53}$$

The gradient with respect to w_{leak}:

$$\begin{aligned}
&\frac{\mathrm{d}y_t}{\mathrm{d}w_{\text{leak}}} = \frac{\partial y_t}{\partial w_{\text{leak}}}\frac{\mathrm{d}V_t}{\mathrm{d}w_{\text{leak}}} = \\
&= \Theta_1'(V_t - V_{\text{thresh}}) \cdot \\
&\Big[-V_{t-1}\Theta_2(V_{\text{thresh}} - V_{t-1}) - V_{t-2}(1 - w_{\text{leak}})\Theta_2(V_{\text{thresh}} - V_{t-1})\Theta_2(V_{\text{thresh}} - V_{t-2}) - \\
&V_{t-3}(1 - w_{\text{leak}})^2\Theta_2(V_{\text{thresh}} - V_{t-1})\Theta_2(V_{\text{thresh}} - V_{t-2})\Theta_2(V_{\text{thresh}} - V_{t-3}) + \\
&(1 - w_{\text{leak}})^3\Theta_2(V_{\text{thresh}} - V_{t-1})\Theta_2(V_{\text{thresh}} - V_{t-2})\Theta_2(V_{\text{thresh}} - V_{t-3})\frac{\mathrm{d}V_{t-3}}{\mathrm{d}w_{\text{leak}}}\Big] = \\
&\Theta_1'(V_t - V_{\text{thresh}}) \cdot \Big[-\textstyle\sum_{n_1}^{N} V_{t-n}(1 - w_{\text{leak}})^{n-1} \cdot \prod_{i=1}^{n}\Theta_2(V_{\text{thresh}} - V_{t-i})\Big]
\end{aligned} \tag{54}$$

These gradient definitions can be implemented with the following code in tensorflow:

```
@tf.function
def lif_gradient(x, w_i, w_l, t_thresh=1):
    time_steps = x.shape[1]

    Vm = w_i * x[:, 0]
    states = tf.TensorArray(tf.float32, size=time_steps)

    for i in tf.range(time_steps):
        Vm = w_i * x[:, i] + (1 - w_l) * Vm * theta2(t_thresh - Vm)
        spike = theta1(Vm - t_thresh)
        states = states.write(i, spike)

    return tf.transpose(states.stack())
```

With the theta functions defined as:

```
@tf.custom_gradient
def theta2(x):
    def grad(dy):
        return dy*0
    return tf.cast(x > 0, tf.float32), grad

@tf.custom_gradient
def theta1(x):
    def grad(dy):
        return dy*1
    return tf.cast(x > 0, tf.float32), grad
```

In the next step, the LIF unit implementation described above is embedded in a hybrid neural network out of LSTM layers and a softmax layer. This hybrid neural network is applied to an image classification task, where 10 different flower species should be identified. The data set is a sub data set of the 102 category flower data set(Nilsback and Zisserman, 2008). Thus, the LIF units should preprocess and compress the images of the different blossoms.

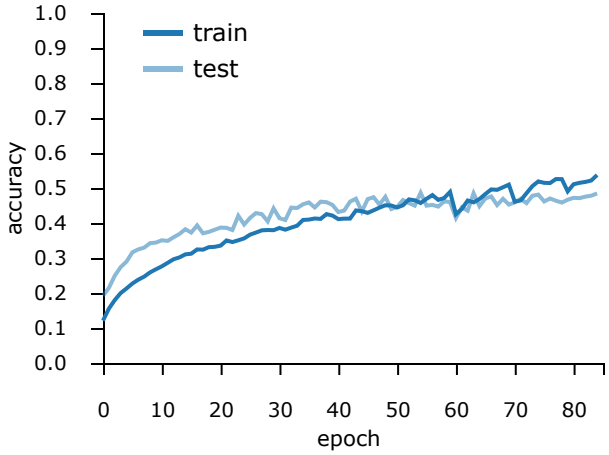

Figure 8: **Accuracy of training a network with a LIF layer;** The training accuracy is shown in dark blue and the test accuracy in light blue.

4.3 LIF Units for Image Classification

4.3.1 Network Architecture 1

The classification task on different blossoms is based on the 10 most occurring flower species of the 102 category flower data set (Nilsback and Zisserman, 2008). The used network consists of one LIF layer with 3 different LIF units types (3x2=6 trainable parameters) compressing the colored images of 500x400 pixels.

The three LIF unit types each get exactly one color channel of the input images. Each LIF unit type receives in each time step one column of one color channel of the image as input and returns a spike vector still representing the same color channel. Thus, the view that the LIF layer consists of 1200 individual LIF neurons of 3 different sorts (in analogy to network architecture 2) with 1D spike train output is equivalent, although for programming reasons the tensor notation was used in the tensorflow (Abadi et al., 2015) implementation.

Thus, the 8 bit images are compressed by a factor of 8 as each 8 bit integer is replaced by a bool number (spike, no spike).

The compressed spike data is fed to an LSTM layer connected to a fully connected output layer with softmax activation. As loss function the categorical cross-entropy is used. The parameters w_{input} and w_{leak} are automatically trained via backpropagation.

The detailed network architecture is give as table:

Layer (type)	Output Shape	Parameters #
LIF-Layer	(None, 400, 500, 3)	6
Reshape	(None, 500, 1200)	0
LSTM Layer	(None, 500, 30)	147720
Dropout	(None, 500, 30)	0
Time distributed Dense	(None, 500, 30)	930
Dropout	(None, 500, 30)	0
Softmax	(None, 500, 10)	310

The training procedure is stopped after 30 epochs of no improvement of the test accuracy ("early stopping"). The figure below shows the training performance as well as the test performance of the described neural network.

The accuracy is defined as the average probability value of the correct label during the image presentation, a very conservative estimator for the accuracy.

The test accuracy achieves a value of over 40 %, whereas the chance accuracy is (10%, 10 categories). This proves that the LIF neurons can be trained by backpropagation so that they operate in a sophisticated parameter range.

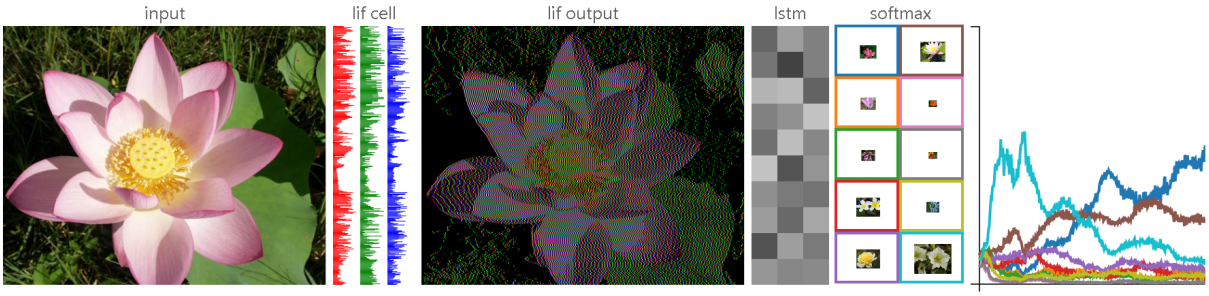

Figure 9: **Spiking network processes images.** The network takes images as input and applies a LIF layer to generate spike trains for each row and color channel. These spike trains are fed into an LSTM layer which is followed by a softmax layer. The softmax layer predicts the category of the image. The categories are represented by images of the training data set, whereas the images used for illustration (input) are part of the test data set. The three different colorbars (lif cell) represent the internal state of the LIF units for the three different color channels. The spike data is produced by this LIF layer is shown under the heading lif output. The activation of the LSTM layer is shown as color map (lstm). The category probability calculated through the softmax layer is represented by the size of the category images (softmax).

The data set does not allow the neural network to train on trivial features such as the color of the flower as the data set contains different color variants of the same flower species.

In the following, we visualize how the network processes the input images and generates a prediction.

The LIF units compress the image, nevertheless the shape of the flowers can still be seen in the processed image.

The here described model proves that spiking layers can be trained for a classification task. In the next section we show that the gradient can also pass the LIF layer to train a preconnected layer.

4.4 Network Architecture 2

Here we provide evidence that a classification network can also be trained, when there is a fully-connected layer preconnected to the LIF layer. The exact network architecture is given in the table:

Layer (type)	Output Shape	Parameters #
Reshape	(None, 500, 1200)	0
TimeDistributed Dense	(None, 500, 1200)	1441200
LIF-Layer	(None, 500, 1200)	2400
LSTM Layer	(None, 500, 30)	147720
Dropout	(None, 500, 30)	0
Time distributed Dense	(None, 500, 30)	930
Dropout	(None, 500, 30)	0
Softmax	(None, 500, 10)	310

Here, the LIF layer consists of 1200 LIF units, generating output spike trains (1D boolean scalar spike train). Each LIF unit receives a weighted sum of $3 \cdot 400$ values as input (3 color channels and 400 as the images consist of 400 rows). The x-coordinate (500 pixels width of the image) is the time axis.

In contrast to the architecture above (network 1), with only 6 trainable parameters except LSTM and softmax layer (3 LIF neuron types, 1200 LIF neurons), this network has 1,441,200 trainable parameters for the preconnected fully-connected layer and 2,400 trainable parameters (w_{input}, w_{leak}) for the 1,200 individual LIF units. The fact that the gradient can pass the LIF units can be seen when analyzing the accuracy as a function of the epochs (learning curve). The accuracy is higher for the LIF units with the activation function gradient ($\Theta_1' = 1$) set to one (blue curves). This is true for training as well as test accuracy.

The figure shows that the test accuracy for the network, where the gradient can pass, is increased by more than 10 % compared to the vanished gradient network (orange curve) and raises up to a value of approximately 55 %. Nevertheless, the accuracy of the vanished gradient network is not 0, as the random connections lead to usable features for the higher layers (LSTM), an effect that was shown in biology as well as in computer science (Dasgupta et al., 2017). In the

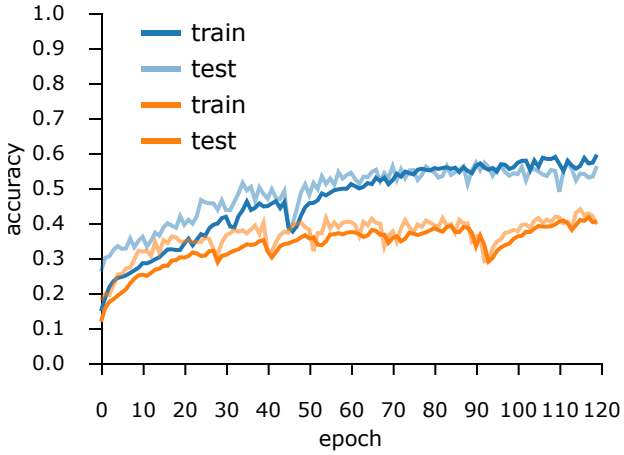

Figure 10: **Accuracy of training a network with a lif layer;** The orange curves show the accuracy course without manually setting the gradient of $\Theta_1' = 1$ (vanished gradient network, dark orange: training accuracy, light orange: test accuracy). The gradient cannot pass the LIF units. The blue curves in contrast show how the algorithm is able to train the LIF layer as well as the preconnected dense layer (dark blue: training accuracy, light blue: test accuracy).

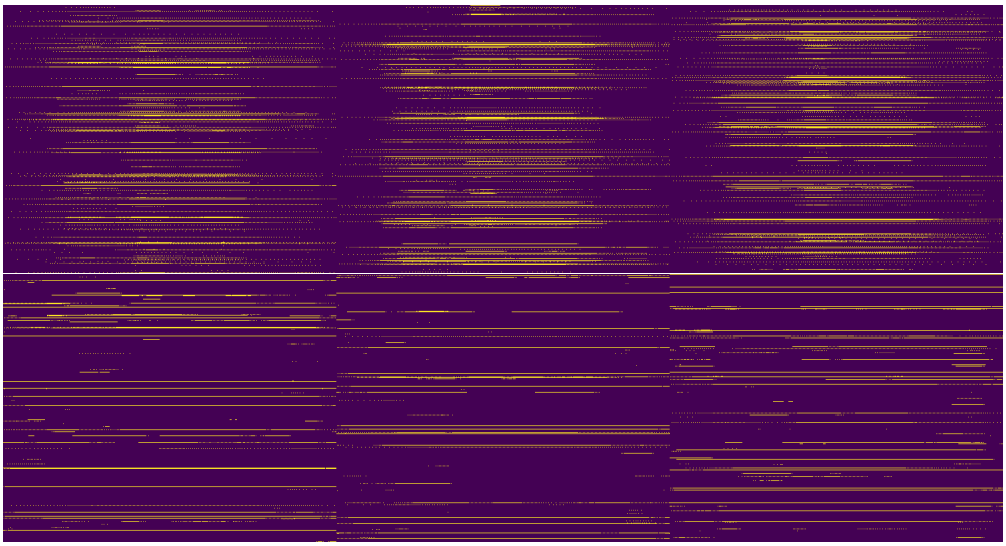

Figure 11: **Training of a network with LIF units.** The figure shows the spiking output of 1200 trained LIF units. Thus, the data was split in 3 blocks only for visualization. Each block consists of 400 lines, which correspond to 400 LIF outputs. The x-axis is the time axis (for each block individually, each block consists 500 time points). The output of each LIF unit is a boolean scalar, which changes over time (x-axis). The input of one LIF unit in each time step is a weighted sum of the rows of the image (each image has 400 rows and 3 color channels, input: weighted sum of 1200 values). It can be seen that the output spike patterns change during training (upper image, epoch 0, lower image epoch 172) and that the spike density is reduced. Thus, the network develops a sparse coding of the input image.

following we show, that the output of the LIF layer significantly changes over the training epochs. Thus, the time course of the output of a LIF unit for one certain image is shown:

The figure provides evidence that the spike patterns clearly change during the training process. This effect is correlated with a higher performance of the network and shows that the gradient can pass the LIF layer.

5 Discussion

5.1 Summary

In this study, we have done an in-depth analysis of the maths behind and the applicability of LIF neurons in Machine Learning applications.

We have shown that parameter tuned LSTM units can show similar spiking patterns as the LIF units. Furthermore, we have provided evidence that LIF units can be embedded in standard neural network models and can be trained with backpropagation. We developed a definition of the gradient, that allows the backpropagated error of a spike to be assigned to those inputs that contributed to this spike. This was done by fixing the derivatives of the activation functions ($\Theta_1' = 1$, $\Theta_2' = 0$).

For our analysis we chose a complex image data set, which has in contrast to simpler data sets such as MNIST, more different frequencies, which translate into different spiking patterns. Up to now, in most studies only simpler data sets were used (Tavanaei et al., 2019).

5.2 Limitations

Although, the LIF units can be trained with backpropagation we are aware of the fact that especially for image classification standard convolutional neural networks perform better.

Additionally, the implementation of recurrent neural networks have to be optimized for the hardware components (Bhuiyan et al., 2010) to increase training speed.

Nevertheless, our results indicate that spiking neural networks are a target to improve Machine Learning as they are energy efficient in hardware implementations (Tavanaei et al., 2019) and have the potential to provide novel insights in the function of biological neural networks(Schemmel et al., 2006; Jin et al., 2010).

5.3 Concluding Remarks

We are convinced that the implementation of biological principles in Machine Learning such as sparsity (Gerum et al., 2019) or spiking properties can help to improve the performance of Machine Learning algorithms. Furthermore, we hypothesize that spiking neural networks could even generate more benefit in applications with serial data such as speech signals (Schilling et al., 2020).

References

Abadi, M., Agarwal, A., Barham, P., Brevdo, E., Chen, Z., Citro, C., Corrado, G. S., Davis, A., Dean, J., Devin, M., Ghemawat, S., Goodfellow, I., Harp, A., Irving, G., Isard, M., Jia, Y., Jozefowicz, R., Kaiser, L., Kudlur, M., Levenberg, J., Mané, D., Monga, R., Moore, S., Murray, D., Olah, C., Schuster, M., Shlens, J., Steiner, B., Sutskever, I., Talwar, K., Tucker, P., Vanhoucke, V., Vasudevan, V., Viégas, F., Vinyals, O., Warden, P., Wattenberg, M., Wicke, M., Yu, Y., and Zheng, X. (2015). TensorFlow: Large-scale machine learning on heterogeneous systems. Software available from tensorflow.org.

Atkinson, K. E. (1989). An introduction to numerical analysis. new york: John willey & sons.

Bhuiyan, M. A., Pallipuram, V. K., Smith, M. C., Taha, T., and Jalasutram, R. (2010). Acceleration of spiking neural networks in emerging multi-core and gpu architectures. In *2010 IEEE International Symposium on Parallel & Distributed Processing, Workshops and Phd Forum (IPDPSW)*, pages 1–8. IEEE.

Burkitt, A. N. (2006). A review of the integrate-and-fire neuron model: I. homogeneous synaptic input. *Biological cybernetics*, 95(1):1–19.

Chollet, F. (2018). *Deep Learning mit Python und Keras: Das Praxis-Handbuch vom Entwickler der Keras-Bibliothek*. MITP-Verlags GmbH & Co. KG.

Dasgupta, S., Stevens, C. F., and Navlakha, S. (2017). A neural algorithm for a fundamental computing problem. *Science*, 358(6364):793–796.

Dominguez-Morales, J. P., Jimenez-Fernandez, A., Rios-Navarro, A., Cerezuela-Escudero, E., Gutierrez-Galan, D., Dominguez-Morales, M. J., and Jimenez-Moreno, G. (2016). Multilayer spiking neural network for audio samples classification using spinnaker. In *International Conference on Artificial Neural Networks*, pages 45–53. Springer.

Field, G. D., Uzzell, V., Chichilnisky, E., and Rieke, F. (2019). Temporal resolution of single-photon responses in primate rod photoreceptors and limits imposed by cellular noise. *Journal of neurophysiology*, 121(1):255–268.

Gers, F. A. and Schmidhuber, E. (2001). Lstm recurrent networks learn simple context-free and context-sensitive languages. *IEEE Transactions on Neural Networks*, 12(6):1333–1340.

Gers, F. A. and Schmidhuber, J. (2000). Recurrent nets that time and count. In *Proceedings of the IEEE-INNS-ENNS International Joint Conference on Neural Networks. IJCNN 2000. Neural Computing: New Challenges and Perspectives for the New Millennium*, volume 3, pages 189–194. IEEE.

Gerum, R. C., Erpenbeck, A., Krauss, P., and Schilling, A. (2019). Sparsity through evolutionary pruning prevents neuronal networks from overfitting. *arXiv preprint arXiv:1911.10988*.

Gross, G. W. and Kowalski, J. M. (1999). Origins of activity patterns in self-organizing neuronal networks in vitro. *Journal of Intelligent Material Systems and Structures*, 10(7):558–564.

Hassabis, D., Kumaran, D., Summerfield, C., and Botvinick, M. (2017). Neuroscience-inspired artificial intelligence. *Neuron*, 95(2):245–258.

Herculano-Houzel, S. (2009). The human brain in numbers: a linearly scaled-up primate brain. *Frontiers in human neuroscience*, 3:31.

Hochreiter, S. and Schmidhuber, J. (1997). Long short-term memory. *Neural computation*, 9(8):1735–1780.

Hodgkin, A. L. and Huxley, A. F. (1952). A quantitative description of membrane current and its application to conduction and excitation in nerve. *The Journal of physiology*, 117(4):500–544.

Izhikevich, E. M. and FitzHugh, R. (2006). Fitzhugh-nagumo model. *Scholarpedia*, 1(9):1349.

Jin, X., Lujan, M., Plana, L. A., Davies, S., Temple, S., and Furber, S. B. (2010). Modeling spiking neural networks on spinnaker. *Computing in science & engineering*, 12(5):91–97.

Koch, C., Segev, I., et al. (1998). *Methods in neuronal modeling: from ions to networks*. MIT press.

Koopman, A., Van Leeuwen, M., and Vreeken, J. (2003). Dynamic neural networks, comparing spiking circuits and lstm.

Krauss, P., Metzner, C., Schilling, A., Schütz, C., Tziridis, K., Fabry, B., and Schulze, H. (2017). Adaptive stochastic resonance for unknown and variable input signals. *Scientific reports*, 7(1):1–8.

Krauss, P., Metzner, C., Schilling, A., Tziridis, K., Traxdorf, M., Wollbrink, A., Rampp, S., Pantev, C., and Schulze, H. (2018). A statistical method for analyzing and comparing spatiotemporal cortical activation patterns. *Scientific reports*, 8(1):1–9.

Krauss, P., Tziridis, K., Metzner, C., Schilling, A., Hoppe, U., and Schulze, H. (2016). Stochastic resonance controlled upregulation of internal noise after hearing loss as a putative cause of tinnitus-related neuronal hyperactivity. *Frontiers in neuroscience*, 10:597.

Kriegeskorte, N. and Douglas, P. K. (2018). Cognitive computational neuroscience. *Nature neuroscience*, 21(9):1148–1160.

Mar, R. A. (2004). The neuropsychology of narrative: Story comprehension, story production and their interrelation. *Neuropsychologia*, 42(10):1414–1434.

Nilsback, M.-E. and Zisserman, A. (2008). Automated flower classification over a large number of classes. In *2008 Sixth Indian Conference on Computer Vision, Graphics & Image Processing*, pages 722–729. IEEE.

Perkel, D. H. and Bullock, T. H. (1968). Neural coding. *Neurosciences Research Program Bulletin*.

Pontes-Filho, S. and Nichele, S. (2019). Towards a framework for the evolution of artificial general intelligence. *arXiv preprint arXiv:1903.10410*.

Rahwan, I., Cebrian, M., Obradovich, N., Bongard, J., Bonnefon, J.-F., Breazeal, C., Crandall, J. W., Christakis, N. A., Couzin, I. D., Jackson, M. O., et al. (2019). Machine behaviour. *Nature*, 568(7753):477–486.

Rieke, F. and Baylor, D. A. (1998). Single-photon detection by rod cells of the retina. *Reviews of Modern Physics*, 70(3):1027.

Russakovsky, O., Deng, J., Su, H., Krause, J., Satheesh, S., Ma, S., Huang, Z., Karpathy, A., Khosla, A., Bernstein, M., et al. (2015). Imagenet large scale visual recognition challenge. *International journal of computer vision*, 115(3):211–252.

Schemmel, J., Grubl, A., Meier, K., and Mueller, E. (2006). Implementing synaptic plasticity in a vlsi spiking neural network model. In *The 2006 IEEE International Joint Conference on Neural Network Proceedings*, pages 1–6. IEEE.

Schilling, A., Gerum, R., Zankl, A., Schulze, H., Metzner, C., and Krauss, P. (2020). Intrinsic noise improves speech recognition in a computational model of the auditory pathway. *bioRxiv*.

Sheng, Y.-B. and Zhou, L. (2017). Distributed secure quantum machine learning. *Science Bulletin*, 62(14):1025–1029.

Shevlin, H., Vold, K., Crosby, M., and Halina, M. (2019). The limits of machine intelligence: Despite progress in machine intelligence, artificial general intelligence is still a major challenge. *EMBO reports*, 20(10):e49177–e49177.

Steinkraus, D., Buck, I., and Simard, P. (2005). Using gpus for machine learning algorithms. In *Eighth International Conference on Document Analysis and Recognition (ICDAR'05)*, pages 1115–1120. IEEE.

Tavanaei, A., Ghodrati, M., Kheradpisheh, S. R., Masquelier, T., and Maida, A. (2019). Deep learning in spiking neural networks. *Neural Networks*, 111:47–63.

Tenenbaum, J. B., Griffiths, T. L., and Kemp, C. (2006). Theory-based bayesian models of inductive learning and reasoning. *Trends in cognitive sciences*, 10(7):309–318.

Thorpe, S., Delorme, A., and Van Rullen, R. (2001). Spike-based strategies for rapid processing. *Neural networks*, 14(6-7):715–725.

Yang, T., Wang, H., Aziz, S., Jiang, H., and Peng, J. (2018). A novel method of wind speed prediction by peephole lstm. In *2018 International Conference on Power System Technology (POWERCON)*, pages 364–369. IEEE.